Magnon dispersion in Ni/Co multilayers grown on Cu(100)

H. Ibach[1,2,*] and C. M. Schneider[1,2,3]
[1]*Peter Grünberg Institut (PGI-6), Forschungszentrum Jülich, 52425 Jülich, Germany*
[2]*Jülich Aachen Research Alliance, Germany*
[3]*Fakultät f. Physik, Universität Duisburg-Essen, 47057 Duisburg, Germany*

(Received 12 March 2019; published 9 May 2019)

Motivated by recent studies on current-driven domain-wall motion we have explored the dispersion of spin waves (magnons) in ultrathin nickel/cobalt multilayers. The layers are grown epitaxially on Cu(100) surfaces and consist of n nickel single-atom layers, each topped by a cobalt bilayer with $n = 2$, 3, and 4 ($n \times Ni_1Co_2$). Layers of the type $2 \times Ni_2Co_1$ are also studied. While parallel to the film plane the magnon dispersion is nearly equal to that of pure cobalt films, magnons with wave vectors perpendicular to the film plane (standing waves) are considerably softened. The softening is attributed to a reduction of the effective interlayer exchange coupling between the two layers next to the interface with the Cu(100) substrate.

DOI: 10.1103/PhysRevB.99.184406

I. INTRODUCTION

Multilayers consisting of a sequence of ultrathin nickel and cobalt layers are known to exhibit strong perpendicular magnetic anisotropy and were therefore considered among other candidates as media for perpendicular recording [1–3]. The interest in these materials was renewed in the context of electronic devices based on current-induced domain-wall motion [4–6] such as racetrack memories [7] and domain-wall logics [8]. The motivation came from theoretical studies which indicated a significantly lower current density required for domain-wall motion in materials with perpendicular magnetic anisotropy [9–11].

For an atomistic understanding of spin-orientation phenomena in thin Ni/Co films a precise control of the composition and morphology on an atomic level is needed, which may be achieved through epitaxial layer-by-layer growth. The technique enables both the specification of the thickness of the individual Ni- and Co layers in terms of atom layers and the interface quality, which is contrary to most application-motivated studies on domain-wall motion in Ni/Co nanowires [11].

Two types of well-ordered Ni/Co films can be prepared by epitaxial growth: Hexagonal layers with (0001) planes are obtained on W(110) surfaces [12,13]. Ordered layers of nickel and cobalt as well as Ni/Co multilayers exposing a (100) surface plane grow on Cu(100) surfaces. The film structure is akin to fcc, however with a small tetragonal distortion along the vertical axis which depends on the distance to the interface to copper [14,15].

Using spin-polarized low-energy microscopy, Suzuki *et al.* have studied the magnetic domains of hexagonal close-packed multilayers of nickel and cobalt [12] to find perpendicularly polarized domains for $n \times [Ni_2Co_1]$ layers if $n > 3$. Spin orientation, the domain sizes, and shapes of domain walls were found to depend critically on the sequence and number of atom layers in the nickel/cobalt films. The pattern of spin orientation and domain shapes is more complex than in layers which consist solely of either cobalt or nickel. In general, the easy axis of magnetization in thin film rests on magnetocrystalline, interface, and surface, as well as on shape anisotropies. The thickness and roughness of domain walls is controlled by the balance of anisotropy and exchange energies. In order to see if a possibly modified exchange coupling across the Ni/Co interfaces contributes to the complex domain pattern it would be useful to have an atomic view exclusively on the exchange energies. That view is conveniently provided by studies of the dispersion of high-momentum magnons [16–20]. Magnons of higher momentum are controlled by the energy required to rotate an atomic spin with respect to the neighboring atoms. This energy is two to three orders of magnitude larger than the energy per atom required to rotate the spin orientation of a domain with respect to a given crystal direction.

In a previous study we have shown that magnons in ultrathin nickel and cobalt films have nearly the same dispersion when the wave vector is oriented within the film plane. However, perpendicular to the film plane magnons in nickel are softer and more strongly damped compared to cobalt [17]. This paper now focuses on the role of Ni/Co *interfaces* on the spin dynamics in Ni/Co films grown on Cu(100). The films consist of sequences of Ni single-atom layers (Ni_1) followed by two-atom layers of cobalt (Co_2); hence films of the type $n \times (Ni_1Co_2)$ with $n = 2$, 3, and 4. Furthermore, a film containing twice as much Ni as Co, namely a $2 \times Ni_2Co_1$ film is studied for comparison.

We find that magnons in $n \times (Ni_1Co_2)$ films with wave vectors parallel to the film plane (acoustic modes) have about the same stiffness as pure cobalt films. Magnons with a wave-vector component perpendicular to the film plane (standing modes) are significantly softer compared to pure cobalt films. The entire set of dispersion curves is quantitatively fitted by a nearest-neighbor Heisenberg model involving only two exchange-energy parameters: one for the weak exchange

*h.ibach@fz-juelich.de

coupling between the Ni layer adjacent to copper and the next (cobalt) layer above, a second one for all other nearest-neighbor couplings. In particular we find that the interlayer coupling between Ni and Co layers inside the film is as in pure cobalt films. Hence, no significant modification of the exchange coupling arises from the Ni/Co interfaces inside the $n \times (Ni_1Co_2)$ films. The softening of the magnons perpendicular to the $n \times (Ni_1Co_2)$ films compared to pure cobalt films is therefore caused by the strong interaction of the last Ni layer with the Cu(100) substrate.

II. EXPERIMENT

Magnon dispersion in the high-momentum range is measured using inelastic scattering of electrons off the surface of magnetic films. The technique enables the investigation of magnons in the wave-vector range between 1 and 10 nm^{-1} with an energy resolution of about 2.5 meV presently [18,21,22]. The electron-energy-loss spectrometer used here is of the type described in Refs. [23,24]. Unpolarized electrons are used and no polarization analysis is involved. This has the advantage that the electron-magnon interaction does not depend on the orientation of the spin polarization in the film. Domains with different spin orientation contribute equally to the spectrum. According to Suzuki *et al.* the average domain size is on the order of 50 nm whereas the experiment averages over an area of several mm^2. Hence each spectrum represents an ensemble of differently oriented domains. By using unpolarized electrons the experiment as such does not discriminate vibrations and magnons. It is therefore essential that the sample be free of contaminants like oxygen and carbon.

In all experiments discussed here the electron-impact-energy E_0 is chosen as 2.25 eV. The wave vector parallel to the surface $q_{||}$ is set by the wave-vector conservation which for an energy loss is

$$q_{||} = k^{(f)} \sin(\theta^{(f)}) - k^{(i)} \sin(\theta^{(i)}). \quad (1)$$

Here, $k^{(i)}$ and $k^{(f)}$ are the moduli of k vectors of incident and scattered electrons, respectively, and $\theta^{(i)}$ and $\theta^{(f)}$ are the angles with respect to the normal of the surface. The desired wave vector of the magnon parallel to the surface is chosen by rotation of the sample around the axis vertical to the scattering plane. Spectra are recorded at fixed rotation angle. Since the electron-impact energy is relatively low the true wave vector varies slightly with the magnitude of the energy loss. For example, for $E_0 = 2.25$ eV, a nominal wave vector of $q_{||,nom} = 2\,nm^{-1}$ and an energy loss of 15 meV, the true wave vector is $q_{||} = 1.97\,nm^{-1}$.

Film preparation is performed via electron beam assisted evaporation from cobalt and nickel rods. The thicknesses are calibrated vs the ion current of the evaporator, which in turn is calibrated by oscillations in the intensity of reflected 3-keV electrons at grazing incidence ("medium energy electron diffraction (MEED) oscillations") [19,25,26].

Because of our atomic-scale calibration the thickness of films is specified by the number of single-atom layers throughout the paper. The thickness of nickel and cobalt single-atom layers in thin, pseudomorphic films on Cu(100) are 0.17 and 0.175 nm, respectively [14,27]. The thicknesses vary slightly with the position of the layer in the film. The distance between the surface layer and the next layer below, e.g., is contracted by a few percent [14,27].

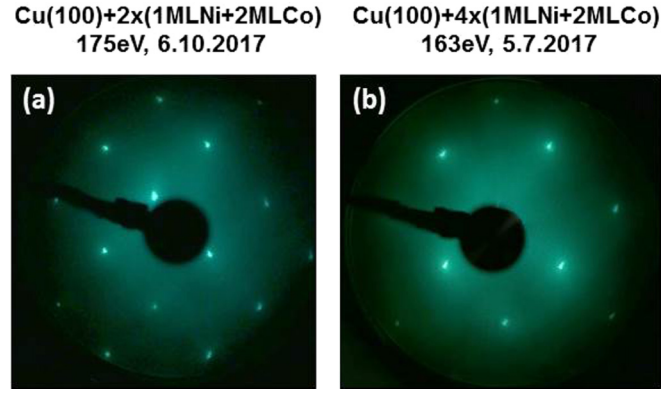

FIG. 1. LEED pattern of (a) $2 \times (Ni_1Co_2)$ film (total of 6 layers) and (b) $4\times(Ni_1Co_2)$ film (total of 12 layers). LEED patterns were taken at slightly different energies (175 and 163 eV for (a) and (b), respectively).

After deposition, the films are annealed to temperatures up to 450 K for 15 min. At this temperature the surface diffusion of cobalt atoms across steps is large enough to initiate smoothening of the surface and thereby a reduction of the density of surface steps. As shown in Ref. [18] this procedure produces flatter surfaces while still no copper creeps to the surface [28].

The lateral order of the films is probed by low-energy electron diffraction (LEED). As examples, Fig. 1 shows the LEED pattern of two films: (a) a 6-layer film of the type $2 \times (Ni_1Co_2)$ and (b) a 12-layer film of the type $4\times(Ni_1Co_2)$. The diffraction patterns demonstrate that both films are well ordered.

III. RESULTS

Characteristic energy-loss spectra for $2 \times (Ni_1Co_2)$ and $2 \times (Ni_2Co_1)$ are displayed in Fig. 2. The impact energy is 2.25 eV; the nominal wave vector is $q_{||} = 1.8\,nm^{-1}$ oriented along the [011] ($\bar{\Gamma}$ $\bar{X}$) direction. The intensity of energy loss and gain features in energy-loss spectroscopy are proportional to $\bar{n} + 1$ and $\bar{n}$, respectively, with $\bar{n} = 1/[\exp(\hbar\omega/k_BT) - 1]$ the Bose occupation number [29]. Here, $\hbar\omega$ is the quantum energy of the loss, T the temperature (300 K), and k_B the Boltzmann constant. By dividing the measured spectra by $(\bar{n} + 1)$ the loss spectra as shown here represent the genuine spectral densities [19].

Both six-layer films, $2 \times (Ni_1Co_2)$ and $2 \times (Ni_2Co_1)$, show two modes. The lower-energy mode is the acoustic mode. The higher-energy mode is the first standing wave [20]. The intensity for the $2 \times (Ni_2Co_1)$ film (blue open squares) is much weaker than the intensity for $2 \times (Ni_1Co_2)$ (blue solid circles). The reason is that electrons interact with magnons practically only via the cobalt atoms. No magnon signals are found in electron scattering from pure nickel films although magnons of nearly the same stiffness as in cobalt exist in these films [17]. To the best of our knowledge the reason for the small cross section with Ni magnons is not fully understood.

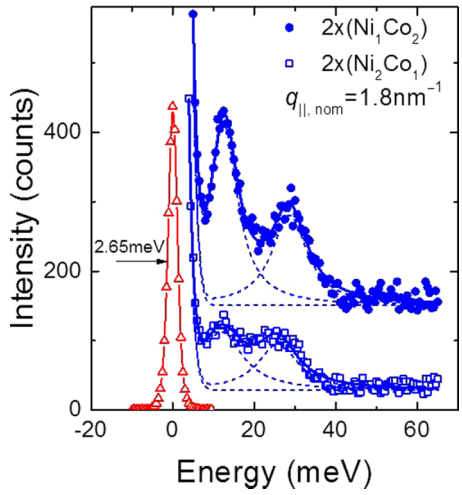

FIG. 2. Magnon spectra for two types of six-atom-layer films: $2 \times (Ni_1Co_2)$ and $2 \times (Ni_2Co_1)$ (solid circles and open squares, respectively). Both spectra are taken with 10 s/channel. The spectrum for $2 \times (Ni_1Co_2)$ is shifted upwards for clarity. The dashed lines denote the decomposition of the spectra into constant background, elastic tail, and Lorentzians.

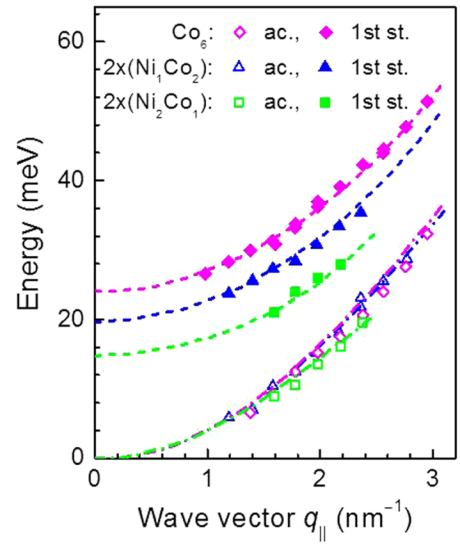

FIG. 3. Magnon dispersion of $2 \times Ni_2Co_1$, $2 \times Ni_1Co_2$ and Co_6 films. The energies of the standing modes of $2 \times Ni_2Co_1$ films (solid green squares) and $2 \times Ni_1Co_2$ films (solid blue triangles) are lower than the standing mode of the Co_6 film (solid magenta diamonds). The stiffness of the acoustic mode of $2 \times Ni_1Co_2$ and Co_6 is identically within the limits of error (open blue triangles and open magenta diamonds, respectively). The stiffness for $2 \times Ni_2Co_1$ appears to be a little lower (open green squares). The lines are the dispersion curves calculated in a nearest-neighbor model (see text for discussion).

One might argue that the cross section should scale with the square of the magnetic moment, from which one would estimate that the electron/magnon interaction in nickel should be about eight times less that in cobalt. However, in reality the electron/magnon cross section in nickel must be even smaller [30].

The solid blue lines in Fig. 2 are fits by a Gaussian for the tail of the elastic peak and two Lorentzians riding on a small constant background. The dashed lines mark the decomposition into the individual peaks. The open red triangles on the left side show the elastic diffuse lines with a full width at half maximum of 2.65 meV. We note that this marks a high resolution achieved in energy-loss spectra of magnons. High-energy resolution is essential: The same spectrum taken with energy resolution of 20 meV would produce a single peak centered at 19 meV instead of two peaks at 12.5 and 28.6 meV. Taking positions of low-resolution magnon spectra vs wave vector would therefore produce bogus dispersion curves in case of several atom layers thick films (compare, e.g., Refs. [31–33]). We remark furthermore that the magnon signals in Fig. 2 are of comparable width as for pure cobalt layers (see Fig. 1 of Ref. [18]).

Neglecting small anisotropy effects and Dzyaloshinskii-Moriya interactions [34,35] the acoustic mode disperses quadratically for small wave vectors $q_{||}$ and therefore approaches zero at $q_{||} = 0$,

$$\hbar\omega = Dq_{||}^2. \tag{2}$$

The parameter D is known as the stiffness. Characteristic for the acoustic mode is the nearly homogeneous precession amplitude across the film. The stiffness of the mode is therefore largely determined by the *intralayer exchange coupling*.

The first standing mode has a node in the precession amplitude situated near the center of the film [26]. Perpendicular to the film plane the amplitude of the mode is approximated by a cosine function with a wave vector

$$q_\perp = \frac{\pi}{Na_\perp}. \tag{3}$$

Here N is the number of layers and $a_\perp$ the interlayer distance. The nonzero perpendicular wave vector causes a nonzero energy at $q_{||} = 0$. The energy at $q_{||} = 0$ approximately scales proportional to N^{-2} and is there entirely determined by the *interlayer exchange coupling*.

Dispersion data for the $2 \times (Ni_2Co_1)$ film are displayed in Fig. 3 (open and solid green squares) together with the data for the $2 \times (Ni_1Co_2)$ film and a six-layer film of pure cobalt. Data points for the acoustic mode of the $2 \times (Ni_2Co_1)$ film (open green squares) appear to fall slightly below the data for $2 \times (Ni_1Co_2)$ and Co_6. The acoustic modes of the $2 \times (Ni_1Co_2)$ film (open blue triangles) and the Co_6 film (open magenta diamonds) have the same stiffness within the limits of error.

Fitting the data for the acoustic mode of the $2 \times (Ni_1Co_2)$ and the Co_6 film to the quadratic dependence [Eq. (2)] we obtain the stiffness as

$$D = 3.9 \text{ meV nm}^2. \tag{4}$$

This value is in good agreement with the stiffness of magnons in bulk fcc cobalt ($D = 3.84$ meV nm^2 [36]) and nickel (3.74 meV nm^{-1} [36–38]). Hence, there is no specific thin-film effect or any noticeable effect of the Ni/Co interfaces on the stiffness of the acoustic mode. This result is consistent with our earlier study on nickel films (equipped with cobalt topping to increase coupling with scattered electrons) [17].

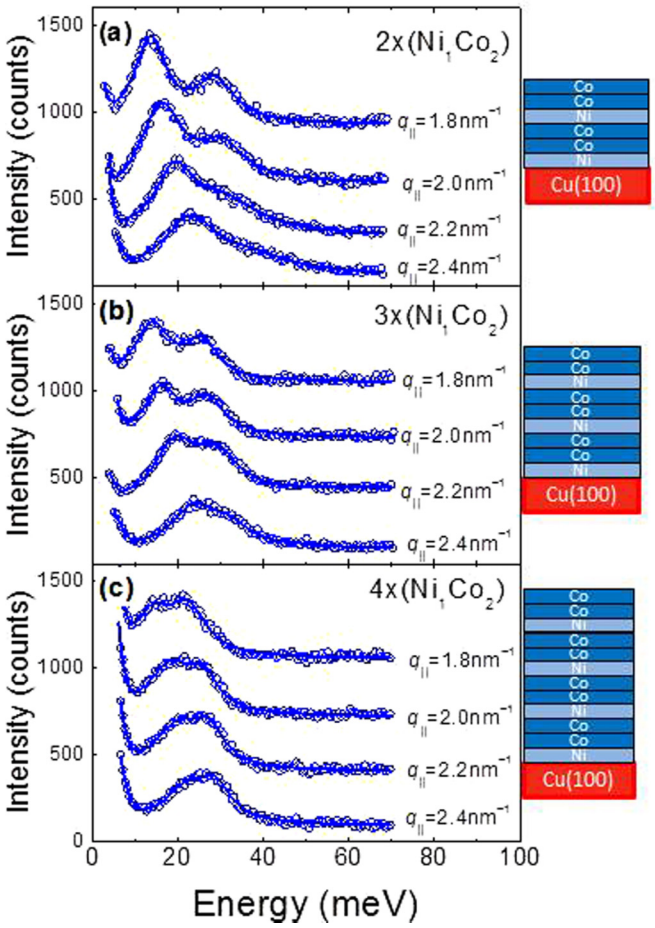

FIG. 4. Magnon spectra for three different films deposited on Cu(100) corrected for the Bose-occupation number: $2 \times (Ni_1Co_2)$, $3\times(Ni_1Co_2)$, and $4\times(Ni_1Co_2)$. Resolution and accumulation time was 4.5 meV and 2 s/channel, respectively. The colored insets show the ideal layer structure.

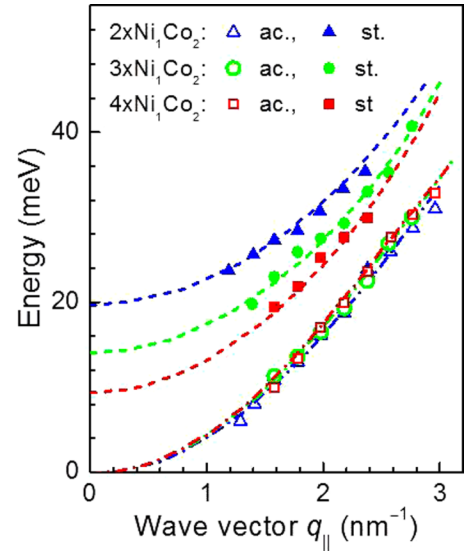

FIG. 5. Magnon dispersion of $n \times Ni_1Co_2$ films for $n = 2$, 3, and 4 are denoted by blue triangles, green circles, and red squares, respectively. Open and solid symbols stand for the acoustic and first standing mode, respectively. The lines map the dispersion curves calculated in a nearest-neighbor model (see text for discussion).

All three six-layer films, Co_6, $2 \times (Ni_1Co_2)$, and $2 \times (Ni_2Co_1)$, have about the same thickness. According to Eq. (3) one would expect the same dispersion of the standing modes if the interlayer exchange-coupling constants of the three films were equal. However, the energies of the standing modes are quite different: data for the $2 \times (Ni_1Co_2)$ film (solid blue triangles) fall significantly below the data for the Co_6 film (solid magenta diamonds). Even lower are the energies of the standing mode in the $2 \times (Ni_2Co_1)$ film (solid green squares). With reference to Eq. (3) we therefore conclude that the exchange coupling at least across one interlayer must be strongly affected by the partial replacement of cobalt with nickel. In order to find out which interlayer exchange coupling is affected mostly we compare the standing modes of $n \times (Ni_1Co_2)$ with $n = 2$, 3, and 4. These films have in common the nickel/copper interface, but differ in the number of nickel/cobalt interfaces.

Figures 4(a), 4(b), and 4(c) show sample spectra for $2 \times (Ni_1Co_2)$, $3\times(Ni_1Co_2)$, and $4\times(Ni_1Co_2)$, respectively. The dispersion data for $n \times (Ni_1Co_2)$ films with $n = 2$, 3, and 4 are compared in Fig. 5. The stiffness of the acoustic modes of the $3\times(Ni_1Co_2)$ film and the $4\times(Ni_1Co_2)$ film (open green circles and open red squares) are equal within the limits of error. The stiffness of the acoustic mode of the $2 \times (Ni_1Co_2)$ film (open blue triangles, same data as in Fig. 3) appears to be slightly lower. The dispersion data of the standing modes in Fig. 5 are marked by solid blue triangles, solid green circles, and solid red squares for the $2 \times (Ni_1Co_2)$, $3\times(Ni_1Co_2)$, and $4\times(Ni_1Co_2)$ film, respectively. The energies are the lower the larger the number of layers is (Eq. (3), see also Ref. [20]). As a consequence, the energies of the acoustic and standing modes merge together with increasing film thickness. Furthermore the modes become the broader the larger their energy is. A separation of the standing mode and the acoustic mode is therefore possible only for small wave vectors $q_{||}$ and small thicknesses.

For the $n \times (Ni_2Co_1)$-type films featuring a smaller interaction between magnons and scattered electrons (Fig. 2) a separation of acoustic and standing modes is achieved only for the $2 \times (Ni_2Co_1)$ film (Figs. 2 and 3).

IV. ANALYSIS OF DISPERSION DATA

In itinerant magnets (Fe, Co, Ni) magnons interact with spin-flip single-electron excitations (Stoner excitations). The interaction leads to Landau damping of magnons as well as to renormalization of magnon energies. In thin films deposited on nonferromagnetic substrates the interaction with Stoner excitations is even stronger as the substrate provides a reservoir of low-energy spin-flip excitations [39–43]. The phase space of Stoner excitations available for interaction with magnons shrinks with decreasing magnon energies and wave vectors. Landau damping therefore decreases rapidly for smaller wave vectors q and levels off to a very small value as q approaches zero [44].

The inclusion of the spectrum of Stoner excitation in a "dynamic theory" of magnons is a challenging task which

has been performed for only a small number of systems and mostly for single-atom layers grown on nonmagnetic substrates [39,43–45]. Remarkably, even the most advanced studies calculate far too high values of the magnon stiffness in case of cobalt layers. The deviation between theory and experiment has been attributed to the fact that theory usually refers to zero temperature [43,46,47] while experiments were mostly performed at higher temperatures. This opinion is however at variance with the experimental fact that no significant temperature dependence of cobalt magnon energies was found between 90 and 300 K [30].

Whereas a theory for magnons in the Ni/Co system is not available, it is useful to analyze the dispersion data within the Heisenberg model. The model (quite incorrectly) assumes that spins localized on neighboring atoms follow the precession of their neighbors adiabatically. Hence, the model neglects the damping of magnons by Stoner excitations and produces δ function like spectral densities. However, the model suffices to describe the dispersion curves as long as the wave vector of the magnon is small.

We consider merely nearest-neighbor interactions as these prevail by about a factor of five to ten in fcc metals [46–48]. We assume the intralayer exchange coupling of cobalt and nickel to be equal. This is a meaningful approach in view of the fact that Co_6, $2 \times (Ni_1Co_2)$, and $2 \times (Ni_2Co_1)$ films have nearly the same stiffness (Fig. 4). Likewise, the stiffness of bulk magnons in fcc cobalt and nickel are close (3.84 vs 3.74 meV nm^{-1} [36–38]). For the moment we assume furthermore that also the interlayer exchange-coupling constants are equal. In that case the stiffness of acoustic magnons along the $\overline{\Gamma}\chi$ [1 $\overline{1}$0] direction in an fcc film with (100) surfaces is described by $D = 4Ja^2$ [17,49]. Here, J and a are the exchange interaction and the lateral lattice constant, respectively. The dispersion of the acoustic modes is thus described by

$$\hbar\omega = 4Ja^2q_{||}^2. \tag{5}$$

When applying that model to the $n \times (Ni_1Co_2)$ films one calculates an exchange interaction of $J = 15$ meV from the experimental stiffness [Eq. (4)].

By using the same model now for the standing modes in $n \times (Ni_1Co_2)$ films one finds that the calculated dispersion approximately matches the experimental data for the $4\times(Ni_1Co_2)$ films without further ado, however overestimates grossly the standing mode energy of $2 \times (Ni_1Co_2)$ (Fig. 6). Qualitatively the same discrepancy is found for pure cobalt films (not shown).

The alternative, namely fitting the standing mode of the thinner $2 \times (Ni_1Co_2)$ film with uniform interlayer coupling constants, would require a substantial reduction of the interlayer exchange coupling. Then, however, the dispersion curve for the standing mode in $4\times(Ni_1Co_2)$ would fall well below the experimental data. A consistent modeling of the magnon dispersion of all $n \times (Ni_1Co_2)$ films is therefore not possible with uniform interlayer exchange-coupling constants.

However, a simple modification of the exchange interaction field leads to a quantitative description of the dispersion curves of cobalt as well as $n \times (Ni_1Co_2)$ films. This modification consists of a reduction of the interlayer interaction between the Nth layer at the copper interface and the penultimate layer above (Table I). The dashed- and dash-dotted dispersion curves in Figs. 4 and 5 are calculated with this set of exchange constants. The curves match the experimental data perfectly. For the $n \times (Ni_1Co_2)$ as well as for the Co_6 film it is assumed that the intralayer coupling in the layer adjacent to the copper interface, J_N, is as in the interior of the film (Table I). However, a moderate reduction of J_N would be also consistent with the experimental data and technically would lead to a slightly better fit of the acoustic mode of the $2 \times (Ni_1Co_2)$ film (Fig. 5).

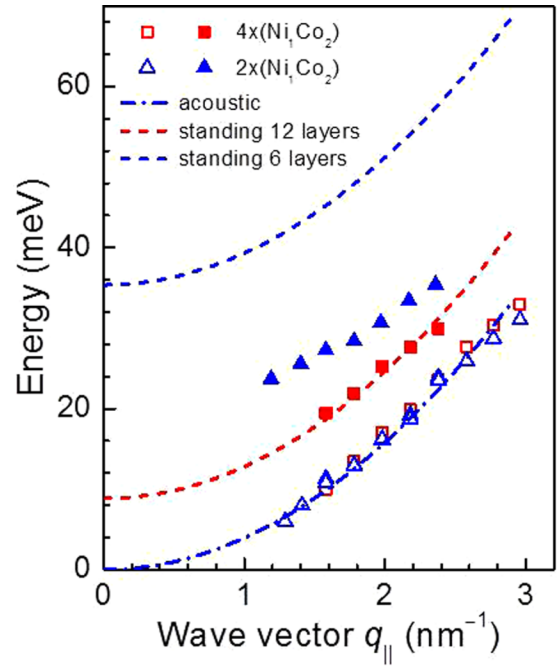

FIG. 6. Dispersion data of $2 \times Ni_1Co_2$ and $4 \times Ni_1Co_2$ films are marked by blue triangles and red squares, respectively. Data are the same as in Fig. 5. The dash-dotted line fits the acoustic mode with a stiffness of 3.9 meV nm^2. The dashed lines are calculated in the nearest-neighbor Heisenberg model assuming homogeneous exchange coupling $J = 15$ meV.

The $2 \times (Ni_2Co_1)$ films feature two Ni layers on top of each other directly at the interface. In that case the stiffness of the acoustic mode is a little smaller than for $2 \times (Ni_1Co_2)$. In addition the standing mode energy is smaller. Matching the experimental data for $2 \times (Ni_2Co_1)$ films in Fig. 3 (green dashed line) requires an additional reduction of $J_{N,N-1}$, and J_N, as well as a mild reduction of J.

TABLE I. Exchange-coupling constants used for the calculation of the dispersion curves in Figs. 4 and 5. Interlayer and intralayer coupling are assumed to be identical except for the interaction between the Nth layer at the interface to Cu(100) and the cobalt layer above denoted as $N - 1$.

	J (meV)	J_N (meV)	$J_{N,N-1}$ (meV)
Co_6	19.5	19.5	3.3
$(2;3;4)\times(Ni_1Co_2)$	19.5	19.5	2.5
$2 \times (Ni_2Co_1)$	18	14	1.8

V. DISCUSSION

The field of exchange interactions considered above deviates qualitatively from the exchange interaction field calculated for cobalt films by Costa *et al.* [48] and Bergqvist *et al.* [46] in the adiabatic model. Neither one features a drastically reduced interlayer exchange constant at the interface. However it is also the case that both exchange interaction fields deviate from each one and neither one as such describes the experimental data of cobalt films [20]. The exchange interaction field of Bergqvist *et al.* only works when globally reduced by about 20% [20]. The discrepancy between theory and experiment is not restricted to fcc films of cobalt. dos Santos *et al.* recently calculated dispersion curves of hexagonal cobalt films on W(110) surfaces using density-functional theory. The theory overvalues the exchange coupling on the average by about 30% (see, e.g., Fig. 10 of Ref. [50]).

Evidence for a significant role of the interface with the substrate on the magnons in 3*d* films is provided by a study of Buczek *et al.* concerning iron, cobalt, and nickel single-atom layers on Cu(100). The authors show that the presence of the substrate causes a reduction of the exchange splitting in the ferromagnetic layer adjacent to copper, a smaller magnetic moment, and a larger energy width of the Stoner continuum [43]. The effect is particular strong for single-atom layers of nickel and gives rise to strong damping and lower magnon energies in the single-layer Ni film. Multilayers were not studied though. The results of Buczek *et al.* nevertheless suggest that the coupling to the substrate has a significant effect on the magnon dispersion. A reduction of the interlayer exchange coupling for layers next to the copper interface as suggested by our analysis of the data is therefore a possible scenario.

VI. CONCLUSION

It is well known from inelastic neutron scattering that bulk nickel and cobalt have comparable strength of the exchange coupling despite the large differences in magnetic moments and Curie temperatures. This study shows that also the exchange coupling between nickel and cobalt across a nickel/cobalt interface is of the same magnitude. The differences in the magnon spectra of Co_6, $n \times (Ni_1Co_2)$, and $2 \times (Ni_2Co_1)$ films are attributed to the interface with the Cu(100) substrate. In particular, the interlayer coupling between the layer directly at the interface and the penultimate layer is strongly affected by the presence of the interface. The interface effect is found to be stronger for nickel than for cobalt, which is consistent with theory [43].

We remark that the experimental data are not at variance with a reduced intralayer coupling in the layer adjacent to the interface. We did not invoke a reduction of the intralayer coupling at the interface since fitting an additional parameter would lack uniqueness.

We finally conclude that the dramatic changes in the domain patterns of Ni/Co films as function of thickness found by Suzuki *et al.* [12] are to be attributed to anisotropies induced by the Ni/Co interfaces and not to interface-induced modifications of the exchange coupling.

ACKNOWLEDGMENTS

The authors have benefited from discussions with A. Ernst, S. Lounis, M. dos Santos Dias, F. dos Santos, and S. Blügel. The able technical assistance of Bernd Küpper, Arnd Bremen, and Claudia Steufmehl has been instrumental to the success of this work.

APPENDIX

The appendix describes magnons in the nearest-neighbor Heisenberg model for the (100) slab of an fcc crystal with layer-dependent exchange couplings.

1. General formulation

For the purpose of calculating the dispersion of spin waves, the Heisenberg Hamiltonian may be transformed into the classical equation [49]

$$\mathrm{i}\hbar\dot{S}_i = 2S\sum_j J_{ij}(S_i - S_j). \tag{A1}$$

The index j in the sum runs over all neighbors (here nearest neighbors). The formulation allows for different exchange constants between atoms. This is of interest for layers composed of different atoms. It is useful to replace the indices by number triples

$$i \to \mathbf{l}_{||}, \quad l_z,\ j \to \mathbf{l'}_{||}, l'_z. \tag{A2}$$

Here, $l_{||}$ is a two-dimensional (2D) number denoting the unit cell and l_z denotes the layer number. Equation (1) then becomes

$$\mathrm{i}\hbar\dot{S}_{\mathbf{l}_{||},l_z} = 2S\sum_{\mathbf{l'}_{||},l'_z} J(\mathbf{l}_{||} - \mathbf{l'}_{||};l_z - l'_z)(S_{\mathbf{l}_{||},l_z} - S_{\mathbf{l'}_{||},l'_z}). \tag{A3}$$

For the 2D-periodic slab we introduce the Fourier transform

$$S_{\mathbf{l}_{||},l_z} = A(\mathbf{q}_{||}, l_z)\mathrm{e}^{\mathrm{i}[\mathbf{q}_{||}\bullet\mathbf{r}(\mathbf{l}_{||},l_z)]}. \tag{A4}$$

The amplitude A depends on the wave vector parallel to the surface of the slab $\boldsymbol{q}_{||}$ and the layer l_z. Assuming a periodic time dependence Eq. (A3) becomes

$$\hbar\omega A(\mathbf{q}_{||}, l_z) = 2S\sum_{\mathbf{l'}_{||},l'_z} J(l_z l'_z) \times\{A(\mathbf{q}_{||}, l_z) - A(\mathbf{q}_{||}, l'_z)\mathrm{e}^{\mathrm{i}\mathbf{q}_{||}\bullet[\mathbf{r}(\mathbf{l}_{||},l_z)-\mathbf{r}(\mathbf{l'}_{||},l'_z)]}\}, \tag{A5}$$

This is the starting equation for calculating the spin waves in a particular direction.

2. Spin waves in an fcc (100) slab along the [01$\bar{1}$] direction

We now consider spin waves along the [01$\bar{1}$] direction ($\bar{\Gamma}$ $\bar{\mathrm{X}}$ direction) of the (100) surface of an fcc slab. We write the q vector as

$$\mathbf{q}_{||} = q_x\mathbf{e}_\mathbf{x}. \tag{A6}$$

After introducing a shorthand notation for the amplitudes $A(\mathbf{q}_{||}, l_z)$ one obtains for the first layer the equation

$$\hbar\omega A_1 = 8JS\left\{\begin{array}{l}\frac{1}{2}C_1A_1 - \frac{1}{4}C_1A_1(e^{iqa} + e^{-iqa}) \\ +C_{12}A_1 - \frac{1}{2}C_{12}A_2(e^{iqa/2} + e^{-iqa/2})\end{array}\right\}. \quad \text{(A7)}$$

Here we have introduced exchange constants in the first layer as $J_1 = C_1J$ and between the first- and second-layer atoms as $J_{12} = C_{12}J$.

For the second layer one has

$$\hbar\omega A_2 = 8JS\left\{\begin{array}{l}\frac{1}{2}C_2A_2 - \frac{1}{4}C_2A_2(e^{iqa} + e^{-iqa}) \\ +C_{12}A_2 - \frac{1}{2}C_{12}A_1(e^{iqa/2} + e^{-iqa/2}) \\ +C_{23}A_2 - \frac{1}{2}C_{23}A_3(e^{iqa/2} + e^{-iqa/2})\end{array}\right\}. \quad \text{(A8)}$$

For the third and deeper layers Eq. (8) applies with corresponding $C_{i,j}$. For the Nth layer of an N-layer slab one has the equivalent equation to (A7):

$$\hbar\omega A_N = 8JS\left\{\begin{array}{l}\frac{1}{2}C_NA_N - \frac{1}{4}C_NA_N(e^{iqa} + e^{-iqa}) \\ +C_{N-1,N}A_N \\ -\frac{1}{2}C_{N-1,N}A_{N-1}(e^{iqa/2} + e^{-iqa/2})\end{array}\right\}. \quad \text{(A9)}$$

We introduce a reduced energy $\tilde{E}$ as

$$\tilde{E} = \hbar\omega/8JS. \quad \text{(A10)}$$

The eigenvalue equation is then

$$\begin{pmatrix}\alpha_1 - E & \beta_1 & 0 & & 0 \\ \beta_1 & \alpha_2 - E & \beta_2 & & 0 \\ & & & & \\ 0 & & & \beta_{N-1} & \alpha_N - E\end{pmatrix}\begin{pmatrix}A_1 \\ A_2 \\ A_N\end{pmatrix} = 0, \quad \text{(A11)}$$

with

$$\begin{aligned}\alpha_1 &= 0.5C_1(1 - \cos q_{||}a) + C_{12}, \\ \beta_1 &= -C_{12}\cos q_{||}a/2 \\ \alpha_2 &= 0.5C_2(1 - \cos q_{||}a) + C_{23} + C_{12}, \\ \beta_2 &= -C_{23}\cos q_{||}a/2 \\ \alpha_{n\neq N} &= 0.5C_{n,n}(1 - \cos q_{||}a) + C_{n,n+1} + C_{n,n-1}, \\ \beta_n &= -C_{n,n+1}\cos q_{||}a/2 \\ \alpha_N &= 0.5C_N(1 - \cos q_{||}a) + C_{N-1,N}.\end{aligned} \quad \text{(A12)}$$

[1] G. H. O. Daalderop, P. J. Kelly, and F. J. A. den Broeder, Phys. Rev. Lett. **68**, 682 (1992).
[2] F. J. A. den Broeder, E. Janssen, W. Hoving, and W. B. Zeper, IEEE Trans. Magn. **28**, 2760 (1992).
[3] M. T. Johnson, P. J. H. Bloemen, F. J. A. den Broeder, and J. J. de Vries, Rep. Prog. Phys. **59**, 1409 (1996).
[4] L. Berger, J. Appl. Phys. **55**, 1954 (1984).
[5] G. Tatara and H. Kohno, Phys. Rev. Lett. **92**, 086601 (2004).
[6] A. Yamaguchi, T. Ono, S. Nasu, K. Miyake, K. Mibu, and T. Shinjo, Phys. Rev. Lett. **92**, 077205 (2004).
[7] S. S. P. Parkin, M. Hayashi, and L. Thomas, Science **320**, 190 (2008).
[8] D. A. Allwood, G. Xiong, M. D. Cooke, C. C. Faulkner, D. Atkinson, N. Vernier, and R. P. Cowburn, Science **296**, 2003 (2002).
[9] S.-W. Jung, W. Kim, T.-D. Lee, K.-J. Lee, and H.-W. Lee, Appl. Phys. Lett. **92**, 202508 (2008).
[10] S. Fukami, T. Suzuki, N. Ohshima, K. Nagahara, and N. Ishiwata, J. Appl .Phys. **103**, 07E718 (2008).
[11] S. Fukami, Y. Nakatani, T. Suzuki, K. Nagahara, N. Ohshima, and N. Ishiwata, Appl. Phys. Lett. **95**, 232504 (2009).
[12] M. Suzuki, K. Kudo, K. Kojima, T. Yasue, N. Akutsu, W. A. Diño, H. Kasai, E. Bauer, and T. Koshikawa, J. Phys.: Condens. Matter **25**, 406001 (2013).
[13] K. Kudo, M. Suzuki, K. Kojima, T. Yasue, N. Akutsu, W. A. Diño, H. Kasai, E. Bauer, and T. Koshikawa, J. Phys.: Condens. Matter **25**, 395005 (2013).
[14] K. Heinz, S. Müller, and L. Hammer, J. Phys.: Condens. Matter **11**, 9437 (1999).
[15] L. Gonzalez, R. Miranda, M. Salmeron, J. A. Vergas, and F. Yndurain, Phys. Rev. B **24**, 3245 (1981).
[16] R. Vollmer, M. Etzkorn, P. S. A. Kumar, H. Ibach, and J. Kirschner, Phys. Rev. Lett. **91**, 147201 (2003).
[17] H. Ibach and C. M. Schneider, Phys. Rev. B **98**, 014413 (2018).
[18] E. Michel, H. Ibach, C. M. Schneider, D. L. R. Santos, and A. T. Costa, Phys. Rev. B **94**, 014420 (2016).
[19] E. Michel, H. Ibach, and C. M. Schneider, Phys. Rev. B **92**, 024407 (2015).
[20] J. Rajeswari, H. Ibach, and C. M. Schneider, Phys. Rev. Lett. **112**, 127202 (2014).
[21] J. Rajeswari, H. Ibach, and C. M. Schneider, Phys. Rev. B **87**, 235415 (2013).
[22] E. Michel, H. Ibach, and C. M. Schneider, Surf. Interface Anal. **48**, 1104 (2016).
[23] H. Ibach, J. Rajeswari, and C. M. Schneider, Rev. Sci. Instrum. **82**, 123904 (2011).
[24] H. Ibach and J. Rajeswari, J. Electr. Spectros. Relat. Phenom. **185**, 61 (2012).
[25] J. Rajeswari, H. Ibach, C. M. Schneider, A. T. Costa, D. L. R. Santos, and D. L. Mills, Phys. Rev. B **86**, 165436 (2012).
[26] H. Ibach, Surf. Sci. **630**, 301 (2014).
[27] A. Clarke, G. Jennings, R. F. Willis, P. J. Rous, and J. B. Pendry, Surf. Sci. **187**, 327 (1987).
[28] M. Giesen, F. Schmitz, and H. Ibach, Surf. Sci. **336**, 269 (1995).
[29] H. Ibach and D. L. Mills, *Electron Energy Loss Spectroscopy and Surface Vibrations* (Academic, New York, 1982).
[30] J. Rajeswari, Ph.D. thesis, University of Duisburg, 2013.
[31] T. H. Chuang, K. Zakeri, A. Ernst, Y. Zhang, H. J. Qin, Y. Meng, Y. J. Chen, and J. Kirschner, Phys. Rev. B **89**, 174404 (2014).
[32] Y. Meng, K. Zakeri, A. Ernst, T. H. Chuang, H. J. Qin, Y. J. Chen, and J. Kirschner, Phys. Rev. B **90**, 174437 (2014).
[33] K. Zakeri, T. H. Chuang, A. Ernst, L. M. Sandratskii, P. Buczek, H. J. Qin, Y. Zhang, and J. Kirschner, Nat. Nanotechnol. **8**, 853 (2013).
[34] J.-H. Moon, S.-M. Seo, K.-J. Lee, K.-W. Kim, J. Ryu, H.-W. Lee, R. D. McMichael, and M. D. Stiles, Phys. Rev. B **88**, 184404 (2013).
[35] T. Moriya, Phys. Rev. **120**, 91 (1960).

[36] S. J. Pickart, H. A. Alperin, V. J. Minkiewicz, R. Nathans, G. Shirane, and O. Steinsvoll, Phys. Rev. **156**, 623 (1967).
[37] H. A. Mook and D. M. Paul, Phys. Rev. Lett. **54**, 227 (1985).
[38] R. N. Sinclair and B. N. Brockhouse, Phys. Rev. **120**, 1638 (1960).
[39] R. B. Muniz and D. L. Mills, Phys. Rev. B **66**, 174417 (2002).
[40] R. B. Muniz, A. T. Costa, and D. L. Mills, J. Phys.: Condens. Matter **15**, S495 (2003).
[41] A. T. Costa, R. B. Muniz, and D. L. Mills, Phys. Rev. B **68**, 224435 (2003).
[42] P. Buczek, A. Ernst, and L. M. Sandratskii, Phys. Rev. Lett. **106**, 157204 (2011).
[43] P. Buczek, A. Ernst, and L. M. Sandratskii, Phys. Rev. B **84**, 174418 (2011).
[44] A. T. Costa, R. B. Muniz, and D. L. Mills, Phys. Rev. B **74**, 214403 (2006).
[45] A. T. Costa, R. B. Muniz, J. X. Cao, R. Q. Wu, and D. L. Mills, Phys. Rev. B **78**, 054439 (2008).
[46] L. Bergqvist, A. Taroni, A. Bergman, C. Etz, and O. Eriksson, Phys. Rev. B **87**, 144401 (2013).
[47] M. Pajda, J. Kudrnovský, I. Turek, V. Drchal, and P. Bruno, Phys. Rev. B **64**, 174402 (2001).
[48] A. T. Costa, R. B. Muniz, and D. L. Mills, Phys. Rev. B **70**, 054406 (2004).
[49] D. L. Mills, in *Modern Problems in Condensed Matter Sciences*, edited by M. Agranovitch and R. Loudon (Elsevier Science, Amsterdam, 1984).
[50] F. J. dos Santos, M. dos Santos Dias, and S. Lounis, Phys. Rev. B **95**, 134408 (2017).